Challenges in the direct detection of chirality-induced spin selectivity: investigation of foldamer-based donor/acceptor dyads

Alberto Privitera[1,2]*, Davide Faccio[3], Demetra Giuri[3], Damiano Genovese[3], Francesco Tassinari[4], Liviana Mummolo[3], Mario Chiesa[2], Claudio Fontanesi[4], Enrico Salvadori[2], Andrea Cornia[4], Claudia Tomasini[3]*, Roberta Sessoli[1]*

[1] *Department of Chemistry "U. Schiff" and INSTM Research Unit, University of Florence, Via della Lastruccia 3-13, 50019, Sesto Fiorentino, Italy*

[2] *Department of Chemistry and NIS Centre, University of Torino, Via Pietro Giuria 7, 10125, Torino, Italy*

[3] *Department of Chemistry "Giacomo Ciamician", University of Bologna, Via Selmi 2, 40126, Bologna, Italy*

[4] *Department of Chemical and Geological Sciences and INSTM Research Unit, University of Modena and Reggio Emilia, Via G. Campi 103, 41125, Modena, Italy*

*e-mail: alberto.privitera@unifi.it, claudia.tomasini@unibo.it, roberta.sessoli@unifi.it

Abstract: Over the past two decades, the chirality-induced spin selectivity (CISS) effect was reported in several experiments disclosing a unique connection between chirality and electron spin. Recent theoretical works have highlighted time-resolved Electron Paramagnetic Resonance (trEPR) as a powerful tool to directly detect the spin polarisation resulting from CISS. Because of the absence of interfaces with conducting electrodes, such spectroscopic evidence could provide a clear understanding of how CISS works at the intramolecular level. Experimental results have demonstrated the potential of this approach for detecting a spin-polarised photoinduced electron transfer (ET) in hybrid systems comprising a CdSe quantum dot as an electron donor (D) connected by a chiral linker (χ) to a fullerene derivative as an electron acceptor (A). However, the study of the ET process in fully organic D-χ-A dyads holds tremendous potential for the unambiguous detection of CISS.

Here, we report a first attempt performed using novel D-χ-A dyads, comprising pyrene (D) and fullerene (A) connected by chiral saturated peptide bridges (χ) of different length and electric dipole moment. The dyads are investigated by an array of techniques, including cyclic voltammetry, optical spectroscopies, and trEPR. Despite the promising energy alignment of the electronic levels and the evidence of luminescence quenching, trEPR does not detect a significant ET highlighting the challenges of spectroscopic detection of CISS. However, the analysis allows the formulation of guidelines for the design of chiral organic model systems suitable to directly probe CISS-polarised ET.

1. Introduction

Chirality plays an essential role in several disciplines ranging from life science and chemistry to physics and material science.[1] Most recently, the concept of chirality has received significant attention following the observation of the so-called chirality-induced spin selectivity (CISS) effect.[2] The CISS effect has disclosed a fundamental link between chirality and the spin angular momentum of the electron.[3] In a nutshell, when the electron passes through a chiral molecule or material, transmission is favoured for a certain spin polarisation, which depends on the handedness of the medium.[4-6] This phenomenon is of paramount interest since it can induce high spin polarisation even at room temperature[7] and can set the stage for novel applications in spintronics and quantum information technologies.[8-10]

In the last few decades, the CISS effect has been observed in several phenomena, such as the response of magnet-free spintronic devices,[9, 11] spin-dependent photoluminescence,[12] enantiomeric enrichment,[13] enantiospecific electrochemistry,[14] and spin selectivity in photoelectrochemical water splitting.[15] However, almost all these experiments relied on the fabrication of hybrid interfaces between chiral molecules and inorganic substrates acting as electrodes, thereby providing solely an indirect observation of CISS. Only recently, a few research groups have focused their attention on the direct detection of the CISS effect at the molecular level.[8, 11, 16, 17] In principle, this could be achieved by probing the spin polarisation arising from photoinduced electron transfer (ET) in D-χ-A architectures, where D is an electron donor, A is an electron acceptor, and χ is a chiral bridge.[8, 11, 16] For these studies, time-resolved Electron Paramagnetic Resonance (trEPR) is the technique of choice, as it allows to probe any CISS-dependent signature on the behaviour of the photogenerated radical pairs, including their coherent spin dynamics.[8, 17, 18] Interestingly, trEPR measurements also have great potential for studying CISS in randomly oriented samples.[16] If successful, the direct detection of the CISS effect via EPR spectroscopy will promote the development of a more robust theoretical description of the phenomenon, with no need to model interfaces, and the formulation of clear and handy guidelines for the synthesis of CISS-active materials. Behind the excitement of these promises, however, lays the stark reality. In fact, the quasi-totality of the available results comes from theoretical works,[8, 18, 19] and the very few experimental attempts present in literature are not conclusive yet.[16] The

main challenge originates from the complexity of developing model systems exhibiting at the same time good ET efficiency, effective chiral spin filtering, and charge transfer (CT) states lasting hundreds of ns, as required for trEPR investigation.[16]

Our previous work identified a hybrid organic-inorganic system comprising a CdSe quantum dot (QD) and C_{60} fullerene as D and A, respectively, covalently linked through a saturated oligopeptide helical bridge (χ).[16] Although this architecture looks promising, the photoexcited state of the inorganic QD has complex spin properties. As a result, it is difficult to discriminate whether the observed spin-polarisation arises from a CISS-mediated ET or a standard ET. In parallel to the QD approach, which as of now remains the most investigated one,[11] it is crucial to develop new chiral systems where the inorganic QD is replaced by an organic D. This approach enables not only to simplify the excited state physics of the D, but also to finely tune its properties by chemical modification. In addition, purely organic D-A systems are often characterized by negligible spin-orbit coupling (SOC), whose impact on the spin selectivity of ET can thus be disclosed by comparison.[11, 17]

Here, we prepare and investigate novel D-χ-A systems (from now on called dyads) that combine two key concepts needed for the direct observation of CISS: (1) fully organic D and A moieties with well-defined photophysical properties, namely pyrene (D) and C_{60} fullerene (A); (2) chiral saturated peptide bridges (χ) of different length and electric dipole moment, known to act as efficient spin filters in spintronic devices.[5, 12, 20] With these dyads in hand we investigate the effect of the chiral bridge on the reduction and oxidation potentials of the D and A moieties via cyclic voltammetry (CV). In addition, through a detailed spectroscopic investigation, including time-resolved photoluminescence (trPL) and trEPR experiments, we highlight the strengths and weaknesses of our novel fully-organic dyads. Finally, we propose guidelines for the design of chiral organic model systems suitable for the direct observation of the CISS effect.

2. Experimental section

2.1 Synthesis

Details on the synthesis and characterisation of **Dir-Pyr**, **Dir4**, **Dir10**, **Dir14**, **Inv-Pyr**, **Inv4**, **Inv10**, **Inv-Pyr'**, and **Inv14** are presented in ESI.† See Figure 1 and synthetic schemes S1-S4 for the molecular structures.

2.2 Electrochemical measurements

The cyclic voltammetry (CV) was performed in a classic three electrode cell (WE: glassy carbon, diameter 2 mm; CE: platinum wire; RE: Ag wire). The Ag wire was used as a quasi-reference electrode and calibrated at the end of every experiment against the ferrocenium/ferrocene (Fc$^+$/Fc) redox couple. Experiments were carried out under Ar atmosphere on degassed 1-mM solutions of the compounds in anhydrous DMSO:toluene (1:1 v/v) containing 0.1 M tetrabutylammonium tetrafluoroborate (TBABF$_4$) as electrolyte, using an AUTOLAB PGSTAT type III potentiostat/galvanostat and NOVA software from Metrohm Autolab. The WE was mechanically polished before each experiment with 50 nm alumina, followed by electropolishing.

2.3 Optical measurements

UV−vis absorption spectra were recorded at 25 °C by means of Perkin-Elmer Lambda 45 spectrophotometer. Quartz cuvettes with optical path length of 1 cm were used. The fluorescence spectra were recorded with an Edinburgh FLS920 equipped with a photomultiplier Hamamatsu R928P. The same instrument connected to a PCS900 PC card was used for the trPL experiments, based on the time correlated single photon counting technique (excitation wavelength = λ_{exc} = 330 nm, emission wavelength = λ_{em} = 395 & 465 nm). Luminescence quantum yields (±15% uncertainty) were determined using quinine sulfate in diluted sulfuric acid as a reference (Φ_{PL} = 0.50). Emission intensities were corrected for inner filter effects according to standard methods. The optical measurements were performed in pure DMSO (approximate concentration 5 μM).

2.4 TrEPR measurements

All trEPR spectra were recorded on a Bruker Elexsys E580 X-band spectrometer equipped with a dielectric ring resonator (ER 4118X-MD5). The sample temperature was maintained using a helium gas-flow cryostat Oxford Instruments CF9350 and controlled with an Oxford Instruments ITC503. Laser excitation was provided by a Litron AURORA II opto-parametric oscillator (OPO) tuneable laser (model number: A23-39-21, 21 Hz repetition rate, E/pulse ≈ 2 mJ, λ = 450 nm, pulse duration = 7 ns). The laser beam was coupled to the resonator through an optical window. No effects of laser beam polarisation are detected, which suggests the laser beam is non-polarised at sample position. trEPR experiments were performed by direct detection with the transient recorder without lock-in amplification. The instrument response time was about 200 ns. The spectra were acquired with 2 mW microwave power and averaging 100 transient signals at each field position. The magnetic field was measured with a Bruker ER035M NMR gaussmeter.

The trEPR measurements were performed on four dyads, i.e. **Dir4**, **Inv4**, **Inv10**, and **Inv14**. Different solvents were probed (toluene:DMSO, DMF, and toluene) to test how the solvent affects the ET efficiency. Since no significant differences were detected, in the text we report only the measurements in DMSO:toluene (1:1 v/v), in line with the photophysical and electrochemical studies. To avoid aggregation, the concentration of the solutions was 20 μM. The solutions were poured inside EPR quartz tubes that were sealed with Teflon under dinitrogen atmosphere.

After data acquisition, baseline correction in both time and field dimensions was performed. First, we subtracted the pre-trigger offset for each field point; second, we filtered out the laser-induced background signal by subtracting the off-resonance signal intensity from the spectra at each time point. From the data set obtained, the transient EPR spectrum at different time delays after the laser pulse was extracted. The reported trEPR spectra have been averaged over a time window of 0.2 μs.

3. Results and discussion

3.1 Dyads building blocks

To optimize the photoinduced ET process, which is key for an efficient detection of the CISS effect via trEPR,[16] we engineered our D-χ-A dyads with the pyrene and C_{60} fullerene units acting as D and A, respectively. Pyrene is a very attractive chromophore due to its intrinsic optical properties, such as high photoluminescence (PL) quantum yield, long fluorescence lifetimes, and controlled formation of excimers and aggregates, which made it one of the most studied fluorescent probes in macromolecules and nanostructured systems.[21] In addition, it is an excellent D and has been used as an antenna chromophore in dyads with C_{60} fullerene for solar energy conversion applications.[22-25] Its long singlet lifetime ensures that when pyrene is coupled with an A, the photoinduced ET occurs from a singlet excited state, which significantly simplifies the interpretation of the spin polarisation arising from the ET.[25] C_{60} fullerene has excellent A abilities thanks to its low-lying unoccupied molecular orbitals and the small reorganization energy in the ET process.[26] As a result, C_{60} fullerene derivatives have played a fundamental role in the design of photoactive D-A dyads and triads, and in the organic photovoltaic field.[17, 22, 27-31] Furthermore, the very small spectral overlap between pyrene emission and C_{60} fullerene absorption rules out the possibility of an efficient Fluorescence Resonance Energy Transfer (FRET) from pyrene to C_{60} fullerene, in favour of the ET process.[22]

Turning now to the chiral bridges, peptide chains are known to promote high spin selectivity in CISS-based spintronic devices.[3-5, 12, 20, 32] The chiral bridges used herein are based on the L-Ala-D-Oxd repeating unit, where L-Ala is L-alanine and D-Oxd is the pseudo amino acid (4S,5R)-4-methyl-5-carboxyl-oxazolidin-2-one. These peptides can form well-organized 3_{10} helices when the number of repeating units is higher than five, as demonstrated by the enhancement of the circular dichroism.[33] Different spacer lengths, i.e. 4, 10, and 14 amino acids, were probed to investigate the trade-off between ET and spin filtering efficiency. In addition, since literature results show that the direction of the electric dipole of the bridge can have a profound impact on ET efficiency,[34] two different types of dyads – hereafter referred to as "direct" and "inverse" – were investigated. In "direct" dyads (Dir), the electric dipole of the peptide chain is parallel to the ET direction (from pyrene to C_{60} fullerene), while in inverse dyads (Inv) it is antiparallel. Six different dyads were then designed, namely **Dir4**, **Dir10**, **Dir14**, **Inv4**, **Inv10**, and **Inv14**, where the digit indicates the number of amino acids (Figure 1).
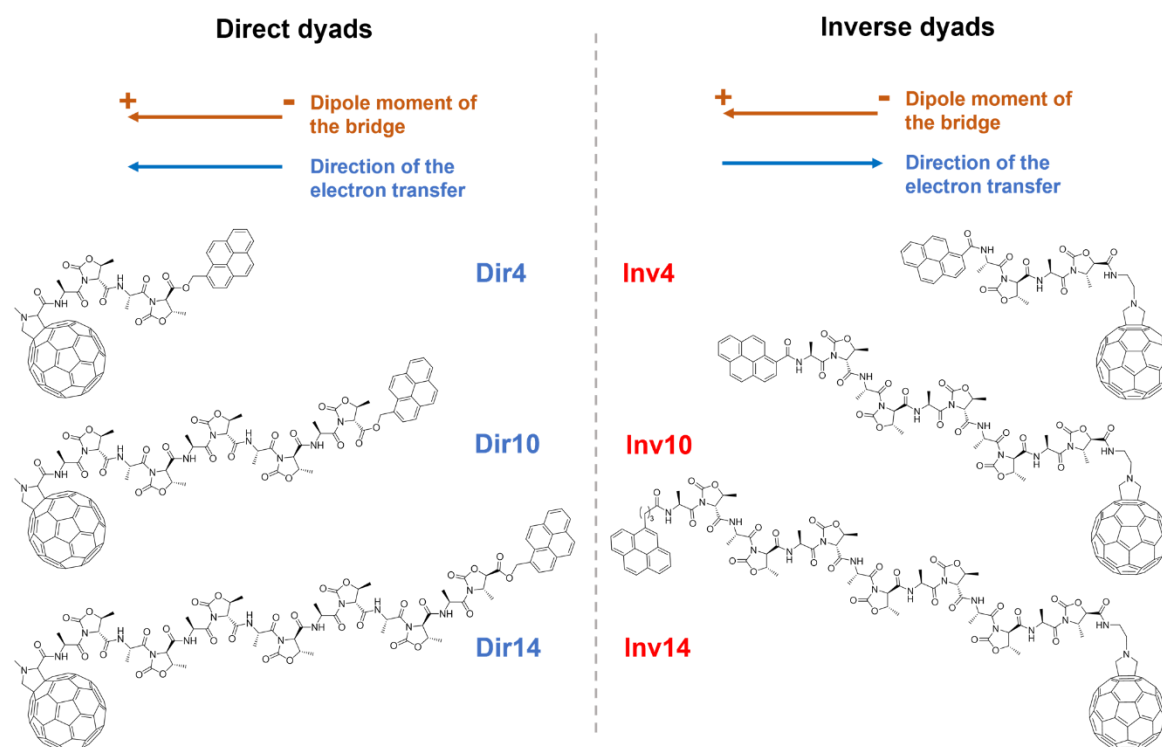

Figure 1 - Engineering of the D-χ-A dyads. Sketched molecular structures of the six D-χ-A dyads synthesised in this work. The pyrene unit acts as an electron donor (D) and the C_{60} fullerene unit as an electron acceptor (A). Different chiral bridges have been probed to investigate the role of the bridge length and its electric dipole moment. Legend: Dir = direct dyad, i.e. the electric dipole moment of the bridge is parallel to the direction of ET; Inv = inverse dyad, i.e. the electric dipole moment of the bridge is antiparallel to the direction of ET; n = number of amino acids of the peptide bridge.

3.2 Synthesis of the dyads

All the molecules were prepared by liquid phase synthesis, starting from commercially available L-alanine, D-threonine, C_{60} fullerene, and pyrene derivatives. The functionalization of C_{60} fullerene was successfully obtained according to the Prato reaction,[35] with either a carboxyl group derivative for direct dyads or an amino group for inverse dyads (Schemes S1-S4). The bridges were prepared by peptide coupling with good to excellent yields.

For the preparation of direct dyads **Dir4**, **Dir10**, and **Dir14**, (*N*-methyl)-fulleroproline *t*-butyl ester was synthesised according to the conditions reported in the literature for similar compounds[35] and coupled with one L-Ala-D-Oxd-OBn unit, forming (*N*-methyl)-fulleroproline-L-Ala-D-Oxd-OBn. The bridges of different length were derivatised, replacing the OBn protecting group with 1-(bromomethyl)pyrene. Finally, the two chains holding the fulleroproline unit at the *N*-terminal position and the pyrene unit at the *C*-terminal position were deprotected and coupled, giving the required dyads, with good yield after careful purification. For further details, chemical yields, and characterizations see ESI (Scheme S1).

To prepare the inverse dyads **Inv4**, **Inv10**, and **Inv14**, C_{60} fullerene was derivatised to Boc-*N*-aminoethyl-*N*-fulleropyrrolidine, following a known procedure,[35] then the *N*-Boc protecting group was removed and replaced with one L-Ala-D-Oxd-OBn unit, to furnish Boc-L-Ala-D-Oxd-*N*-2-aminoethyl-fulleropyrrolidine (Scheme S2). The inverse dyads **Inv4** and **Inv10** were prepared by coupling this derivative with two bridges holding a carboxypyrene group, namely pyrenecarbonyl-L-Ala-D-Oxd-OBn for **Inv4** and pyrenecarbonyl-(L-Ala-D-Oxd)$_4$-OBn for **Inv10**. After removal of the protecting groups, peptide coupling and purification, the two dyads were obtained in good overall yields (Scheme S3). The dyad **Inv14** was prepared in a similar way, coupling Boc-L-Ala-D-Oxd-*N*-2-aminoethyl-fulleropyrrolidine with 4-pyren-1-yl-butanoyl-L-Ala-D-Oxd-OBn. After removal of the protecting groups, peptide coupling and purification, this third inverse dyad was obtained in good overall yield (Scheme S4). For our purposes, the use of a 4-(pyren-1-yl)-butanoate group, replacing the pyrene-1-carboxylate group (used for **Inv4** and **Inv10**) affects the photophysical properties only marginally, as shown below.

Three short-chain control compounds carrying a pyrenyl termination but no fulleryl group were also synthesised and employed as control systems for the electrochemical and photophysical measurements, namely **Dir-Pyr** (Scheme S1), **Inv-Pyr** (Scheme S3), and **Inv-Pyr′** (Scheme S4). **Dir-Pyr** is the control compound for the three direct dyads (**Dir4**, **Dir10**, and **Dir14**), **Inv-Pyr** is the control compound for the short (**Inv4**) and intermediate (**Inv10**) inverse dyads, and **Inv-Pyr′** is the control compound for the long inverse dyad (**Inv14**). Their synthesis and characterization are reported in ESI.

3.3 Electrochemical measurements

CV measurements in DMSO:toluene (1:1 v/v) were performed on **Dir4**, **Inv4**, **Dir10**, and **Inv10** dyads, as well as on the short-chain control compounds **Dir-Pyr** and **Inv-Pyr**. Figure 2 sets out a representative CV, recorded on **Inv4** dyad; the whole set of experimental CVs can be found in the ESI.

The electrochemical response of the fulleryl group is clearly observable in all four dyads, which exhibit three well-differentiated reversible reduction peaks at $E^{(1/2)}_{red1} \sim -0.6$ V, $E^{(1/2)}_{red2} \sim -1.0$ V,

and $E^{(1/2)}_{red3} \sim -1.6$ V (vs. Fc$^+$/Fc, see Table 1). The longer dyads (**Dir10** and **Inv10**) have slightly less negative reduction potentials compared to the shorter ones. All dyads, as well as **Dir-Pyr** and **Inv-Pyr**, exhibit a reversible peak at $E^{(1/2)}_{red4} \sim -2.2$ V that we attribute to the reduction of the pyrenyl group.[36] It has to be noted that the direct attachment of the amide group to the pyrenyl moiety via carbonyl carbon should enhance the electron-accepting properties of the pyrenyl chromophore.[36] Despite this, **Inv4**, **Inv10**, and **Inv-Pyr** show reduction potentials quite similar to those observed in their direct counterparts.
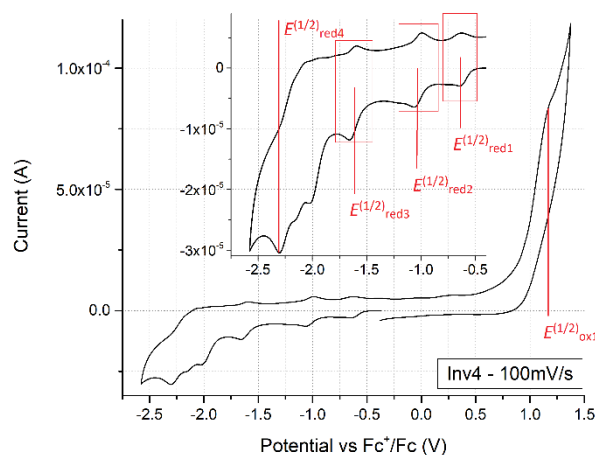

Figure 2 - Representative CV of **Inv4** (1 mM) recorded in anhydrous DMSO:toluene (1:1 v/v) at a scan rate of 100 mV/s with 0.1 M TBABF$_4$ electrolyte.

The anodic portion of the CV is less resolved, and the recorded current values indicate multiple overlapping irreversible oxidation processes that take place at potential values around 1.2 - 1.3 V vs. Fc$^+$/Fc, or just lower. In this potential window, one expects oxidation of both pyrenyl and amide moieties.[36] In particular, in their classical work O'Donnell and Mann report oxidation potentials of 0.8-1.1 and 1.4 V vs. Fc$^+$/Fc for tertiary and secondary aliphatic amides, respectively.[37] The best-defined anodic peak before the onset of solvent oxidation gives $E^{(1/2)}_{ox1} \sim 1.2$ V (Table 1). Combined with the fulleryl $E^{(1/2)}_{red1} = -0.6$ V reduction potential, this yields an electrochemical HOMO-LUMO gap of ca. 1.8 V for the four dyads investigated. The electrochemical HOMO-LUMO gap for pyrenyl group, estimated as $E^{(1/2)}_{ox1} - E^{(1/2)}_{red4}$, is ca. 3.4 V, in agreement with literature data,[36] and matches well the optical bandgap obtained from UV-vis spectra (ca. 3.45 V, in agreement with previous reports).[38, 39] This analysis evidences that the fulleryl LUMO is lower in energy than the pyrenyl LUMO and therefore suggests that the ET process is, in principle, favoured for all the dyads without significant differences between direct and inverse ones or linkers with different length.

Table 1. Half-wave potential values and electrochemical HOMO-LUMO gaps (V) for 1 mM solutions of dyads and control compounds in DMSO:toluene (1:1 v/v) with 0.1 M TBABF$_4$[a]

Compound	$E^{(1/2)}_{red1}$	$E^{(1/2)}_{red2}$	$E^{(1/2)}_{red3}$	$E^{(1/2)}_{red4}$	$E^{(1/2)}_{ox1}$ [b]	$E^{(1/2)}_{ox1} - E_{red1}^{(1/2)}$ [c]	$E^{(1/2)}_{ox1} - E_{red4}^{(1/2)}$ [d]
Dir4	−0.66	−1.09	−1.70	−2.18	1.22	1.88	3.40
Inv4	−0.62	−1.02	−1.62	−2.19	1.17	1.79	3.36
Dir10	−0.58	−1.03	−1.64	−2.18	1.27	1.85	3.45
Inv10	−0.58	−1.02	−1.61	−2.19	1.13	1.71	3.32
Dir-Pyr	-	-	-	−2.14	1.23	-	3.37
Inv-Pyr	-	-	-	−2.18	1.14	-	3.32

[a]*Vs. the Fc⁺/Fc redox couple.* [b]*Estimated from the inflection points of the anodic waves for the irreversible oxidation peaks.* [c]*Electrochemical HOMO-LUMO gap for the dyad.* [d]*Electrochemical HOMO-LUMO gap for pyrenyl group.*

3.4 Photophysical measurements

We investigated the photophysical properties of our samples in solution by combining UV-vis absorption and PL spectroscopy (Figures 3 and S9). We carried out the measurements in pure DMSO, which is a better solvent for the dyads with respect to chlorinated solvents, DMF, toluene, and other non-polar media. UV-vis spectra of both the direct and inverse dyads show the characteristic absorption bands of pyrene and C$_{60}$ fullerene. These spectra thus suggest that the D/A units have independent optical absorptions,[22] likely as a consequence of the hindered electronic communication between the two terminal chromophores through a peptide bridge. The result is further corroborated by PL spectra, which show the dominant emission of the pyrene unit, as expected based on the relative PL efficiency between pyrene and C$_{60}$ fullerene. In addition to pyrene emission, the PL spectra of **Dir4** and **Dir10** (Figure 3a) feature a significant broad band centred at longer wavelengths (~ 470 nm) and ascribable to the presence of aggregates arising from the poor solubility of these dyads. Indeed, the formation of excimers and aggregates of pyrene can be easily monitored via the clear fingerprint of their red-shifted broad emission, often associated with a multiexponential PL decay.[40] Conversely, **Dir14** and all the inverse dyads show purely monomeric emission spectra without traces of excimers or aggregates (Figure 3b).

To gain further insight into the photophysics of the dyads in solution and probe any photoinduced ET between the pyrene and C$_{60}$ fullerene units, we measured PL quantum yields (Φ_{PL}) and performed trPL experiments on all dyads and the three control compounds. The data in Table 2 reveal that PL quenching is stronger in the three direct dyads (Φ_{PL} = 0.016, 0.004, and 0.030 in **Dir4**, **Dir10**, and **Dir14**, respectively) than in the corresponding control compound **Dir-Pyr** (Φ_{PL} = 0.25). The PL quantum yield is reduced less dramatically in the inverse dyads **Inv4** and **Inv10** (Φ_{PL} = 0.20 and 0.30, respectively) compared to **Inv-Pyr** (Φ_{PL} = 0.58), and in **Inv14** (Φ_{PL} = 0.24) vs. **Inv-Pyr′** (Φ_{PL} = 0.33).

To understand whether this quenching is triggered by aggregation or by photoinduced ET, we now focus on the trPL experiments. The PL decay curves of the direct dyads obtained at λ_{em} = 395 nm (i.e., monitoring the monomer emission) show multiexponential kinetics. Quenching of excited states due to electronic interactions in aggregates, including the formation of excimer, is commonly very fast and occurs in the sub-ns time range.[41, 42] This type of fast quenching is observed in dyads **Dir4** and **Dir10**, which also show the excimer emission band typical of aggregation (Figure 3a). In addition, the presence of rise times (τ_{RISE}) falling in the same sub-ns time scale in the trPL of excimer emission monitored at 465 nm further confirms the critical presence of aggregation for these two dyads. This analysis allows confining the effect of quenching due to aggregation to the sub-ns time region and discussing the longest components of trPL in the perspective of quenching due to ET. Specifically, the longest time is τ_1 = 47.5, 51.8, and 80.0 ns for **Dir4**, **Dir10**, and **Dir14**, respectively, to be compared to 84.9 ns for control compound **Dir-Pyr**, which carries no fulleryl group. This may reflect a partial quenching due to the ET occurring through the chiral bridge. According to the amplitudes of these components of the decay, the mentioned ET efficiencies concern only a fraction of dyads amounting to 6%, 9%, and 35% for dyads **Dir4**, **Dir10**, and **Dir14**, respectively. The intermediate time (τ_2 = 8.2, 7.7, and 8.5 ns for **Dir4**, **Dir10**, and **Dir14**, respectively) can be tentatively assigned to an ET process independent from the bridge length, like that expected to occur in folded conformers where D and A are brought in closer contact.

From the trPL analysis of the inverse dyads, we obtain no clear evidence of aggregation, confirming the absence of excimer emission from these samples (Figure 3b). The most significant component of the decay has the same lifetime as the corresponding control compound (τ_1 = 22.0, 22.4, and 79.1 ns in **Inv4**, **Inv10**, and **Inv14** to be compared to 22.5 ns in **Inv-Pyr** and 79.2 ns in **Inv-Pyr′**), suggesting that no quenching due to the ET takes place. However, **Inv4** and **Inv14** show minor quenching contributions with τ_2 = 3.6 ns and 11.2 ns, respectively, that we attribute to at least one molecular conformation exhibiting a moderate quenching due to ET.
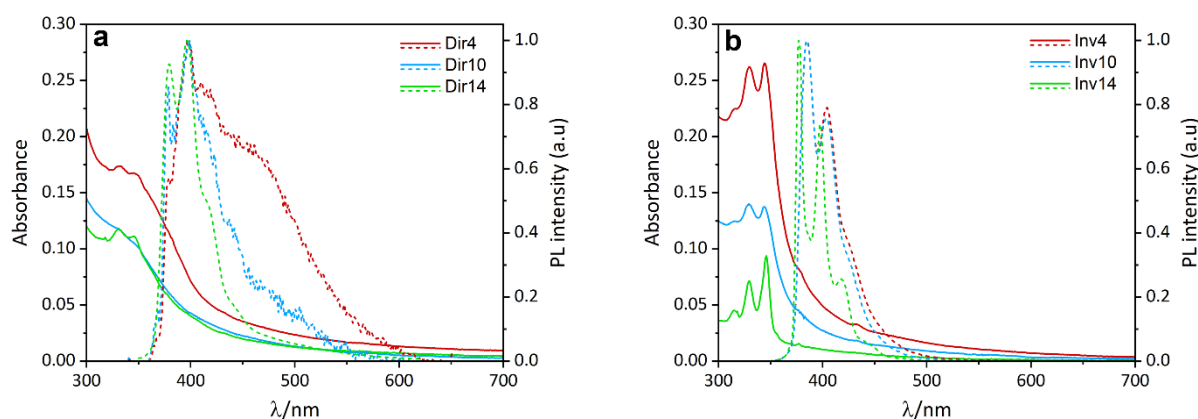
Figure 3 - Absorption and emission spectra of D-χ-A dyads. Absorption (solid lines) and emission spectra (dashed lines) of (a) direct and (b) inverse dyads. Emission spectra were measured with λ_{exc} = 330 nm and normalized at their maximum.

Table 2 - Photoluminescence (PL) quantum yields (Φ_{PL}) and PL lifetimes (τ_n) and amplitudes (B_n) of dyads and control compounds, λ_{exc}=330 nm for both PL quantum yield measurements and trPL experiments; the decay time at λ_{em}=465 nm, τ_{465}, was measured for the dyads **Dir4** and **Dir10** featuring excimer emission band, with rise times τ_{RISE} indicated by the negative amplitude B_{465})

Sample	Φ_{PL}	τ_{395}/ ns (B_{395})	τ_{465} / ns (B_{465})
Dir-Pyr	0.25	τ_1 =84.9	
Dir4	0.016	τ_3 = 0.51 (515) τ_2 = 8.2 (486) τ_1 = 47.5 (63)	τ_{RISE} = 0.15 (-370) $\tau_{Agg,2}$ = 4.6 (496) $\tau_{Agg,1}$ = 17.4 (508)
Dir10	0.004	τ_3 = 0.40 (635) τ_2=7.7 (525) τ_1 = 51.8 (112)	τ_{RISE} = 0.31 (-1286) $\tau_{Agg,2}$ = 4.3 (817) $\tau_{Agg,1}$ = 15.1 (350)
Dir14	0.030	τ_2 = 8.5 (607) τ_1 =80.0 (329)	
Inv-Pyr	0.58	τ_1 =22.5	
Inv4	0.20	τ_2 =3.6 (57) τ_1 =22.0 (892)	
Inv10	0.30	τ_1 =22.4	
Inv-Pyr'	0.33	τ_1 =79.2	
Inv14	0.24	τ_2 =11.2 (112) τ_1 =79.1 (852)	

4.5 TrEPR measurements

We carried out trEPR spectroscopy to elucidate the origin of trPL quenching and evaluate the presence of a spin-polarised photoinduced ET. We performed the measurements on **Dir14** and on the three inverse dyads (**Inv4**, **Inv10**, and **Inv14**) since these four compounds do not show any evidence of aggregation via optical analysis. Aggregation would result in intermolecular ET and therefore impair our analysis. All the dyads were dissolved in DMSO:toluene (1:1 v/v) at 20 μM concentration and photoexcited with a 450 nm laser pulse. All the spectra were acquired at T = 50 K because measurements in fluid solution would undermine the detection of CISS due to motional averaging.[8] In Figure 4, we show the trEPR spectra of the four dyads (black lines) acquired at 1 μs after the laser pulse, along with the spectrum of the CdSe QD-χ-C$_{60}$ system (blue line) studied in our recent publication,[16] as a comparison for the ET. The full 2D experimental trEPR contour plots of the four dyads are available in Figure S11. In all the studied dyads, we observe a broad signal between 335 and 358 mT. Based on the spectral simulation (red line) in Figure 4, we assign this signal to the standard C$_{60}$ triplet state formed via intersystem crossing (ISC) promoted by SOC.[43] However, while the CdSe QD-

χ-C$_{60}$ system exhibits an additional signal due to the photoinduced C$_{60}$ anion,[16] none of the organic dyads do. This observation indicates that a photoinduced ET able to generate a spin-polarised long-lived CT state is not occurring in our fully organic dyads at 50 K.

Both our CV measurements and previous literature results suggest that pyrene/C$_{60}$ should be, in principle, a good D/A couple due to the favourable HOMO-LUMO alignment.[21-23] In addition, our trPL experiments suggest some degree of ET at room temperature for most of the studied dyads. The discrepancy between trPL and trEPR results might be due to the different temperature of the experiments (T = 298 K vs 50 K), as well as to the different sensitivity and time-resolution of the two techniques. One important limitation of trEPR is that it reveals only spin-polarized CT states lasting longer than hundreds of ns.
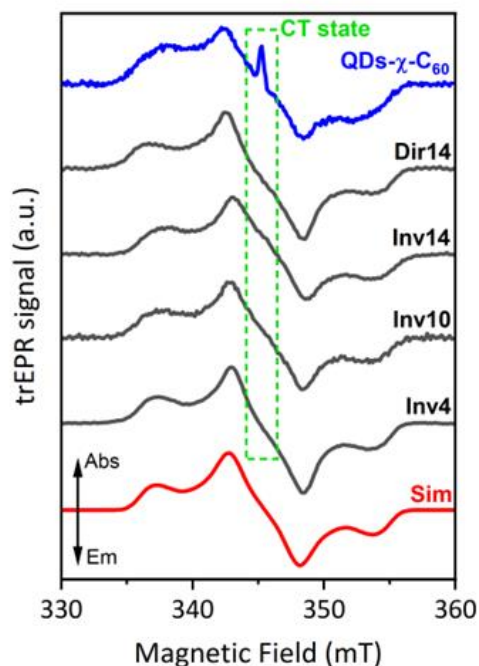
Figure 4 – Time-resolved EPR spectra of D-χ-A dyads. Normalised experimental trEPR spectra of **Inv4**, **Inv10**, **Inv14**, and **Dir14** (black lines) taken at 1 µs after a 450 nm laser pulse (7 ns, 2 mJ). The spectra are acquired at 50 K. All spectra show a broad signal in the magnetic field range 335–358 mT, which is assigned to the C_{60} triplet based on the best-fit spectral simulations (red line). The simulation parameters are reported in Table S1. As a comparison for the ET, the trEPR spectrum of the CdSe QD-χ-C_{60} system (blue line) is also plotted.[16] Arrows legend: Abs = enhanced absorption, Em = emission.

Although peptide helices are known to mediate long-range ET between D/A moieties,[44, 45] to our knowledge multi-technique investigations of this process are unprecedented. Indeed, most literature studies of ET in helical structures were based on optical or electrochemical techniques and mainly aimed at understanding how redox processes occur in biochemical reactions and at controlling them in related synthetic systems.[44-48] As of now, the nature of long-range ET in D-A dyads connected by a peptide bridge is still debated and two different mechanisms have been proposed: (1) a superexchange mechanism, consisting in a coherent electron tunneling in which the peptide bridge tunes the tunneling barrier height and thus the electronic coupling between D and A; (2) a sequential hopping mechanism, consisting in an incoherent, multi-tunneling process that involves the bridge orbitals directly. All studies highlighted the complex nature of the ET process due to several critical parameters, such as the nature of the peptide structure, the hydrogen bonds, the surrounding medium, and conformational fluctuations.[49, 50]

Turning now to the trEPR experiments, most studies on radical pairs generated via photoinduced ET relied on ultrafast multistep ET processes that ensure good ET efficiency and a long lifetime of the photogenerated CT state.[17] Examples can be found in nature, e.g. in photosynthetic reaction center proteins,[51-53] and in D-A-A' triads, where the first charge separation is photodriven, while the second is thermally allowed.[54, 55] Alternatively, good ET efficiencies

and slow recombination rates have been achieved in D-A dyads by finely tuning unsaturated bridges to promote good electronic communication between D and A, while keeping them sufficiently apart to slow down charge recombination.[56] In our case, trEPR measurements do not reveal any sign of ET, likely because the long saturated bridges hinder the electronic communication between D and A.

The failure to detect ET by trEPR, even in the shortest dyads, suggests that our molecular engineering approach to directly probe CISS at the molecular level needs to be deeply reconsidered. Specifically, although most studies on the CISS effect were based on the use of chiral layers containing peptide bridges,[3-6, 9, 11, 12, 20, 57] our results show that new molecular approaches are required to simultaneously achieve good ET efficiencies and efficient CISS-mediated spin filtering in fully organic D-χ-A dyads.

A first approach may rely on *chiral D*-bridge-A dyads, where the CISS filtering potential is provided by D rather than the bridge. This approach could help avoid the constraints imposed by using a saturated chiral bridge, thereby allowing the tuning of the ET efficiency independently from the spin filtering. It would allow playing with different bridge lengths and types to achieve the perfect match between good ET efficiency and slow charge recombination rate. Promising examples of *chiral D*s are helicenes, which have recently shown good spin filtering properties despite their short length.[58-60] In a similar approach, one may envision using a *chiral A*. In this case, following the photoexcitation of A, the spin polarisation would arise from the photoinduced hole transfer from A to D.[17, 27] Another strategy may rely on the use of unsaturated chiral bridges. In this way, the bridge could be engineered to ensure good ET efficiency and slow charge recombination. For instance, aromatic oligoamide foldamers have provided optical evidence of long-distance ET, but no trEPR investigations are reported.[61] Notably, long-lived CT states could also be achieved by the use of D-A'-A triads.[17] All these approaches could help address the fundamental issue of poor ET efficiency observed with the more standard chiral peptides used in the present work. However, limited information regarding the CISS filtering properties of these new chiral moieties is available to date in the literature.

4. Conclusions

In summary, we engineered and synthesised six fully organic D-χ-A dyads comprising pyrene as D and C_{60} fullerene as A. Different chiral peptide bridges (χ) were used to investigate the influence of their length and electric dipole orientation on the spin-polarized ET. Through the combination of cyclic voltammetry, UV-vis absorption, steady-state and time-resolved PL techniques, we characterized our systems with the ultimate aim of probing a CISS-mediated ET *via* trEPR spectroscopy. Although we observed some promising PL quenching, photoinduced ET escaped detection by trEPR, highlighting a critical gap between our novel spectroscopic approach and state-of-the-art experiments for measuring CISS. In particular, while chiral peptides are extensively used in transport measurements, they are inefficient mediators of intramolecular ET when incorporated into fully organic D-χ-A dyads, even those with a highly favourable energy alignment of the D/A pair.

The observation of CISS effect at the intramolecular level by spectroscopic techniques would significantly advance our understanding of the phenomenon. However, our results show that designing suitable molecular architectures is a very demanding task, especially when a fully organic approach is followed so as to gain improved control over photophysical processes. Identifying alternative chiral units that combine efficient ET and good spin filtering ability is a current challenge and a required step to get new insight into the fundamental principles of the CISS effect. In turn, this would help disclose the molecular parameters which underlay effective spin-filtering and promote better engineering of CISS-based molecules and layers needed for the future of CISS-based devices.

Acknowledgements

References

1. A. Guijarro, *The Origin of Chirality in the Molecules of Life: From Awareness to the Current Theories and Perspectives of this Unsolved Problem*, Royal Society of Chemistry, 2022.
2. K. Ray, S. P. Ananthavel, D. H. Waldeck and R. Naaman, *Science*, 1999, **283**, 814-816.
3. R. Naaman, Y. Paltiel and D. H. Waldeck, *Nat. Rev. Chem.*, 2019, **3**, 250-260.
4. R. Naaman, Y. Paltiel and D. H. Waldeck, *J. Phys. Chem. Lett.*, 2020, **11**, 3660-3666.
5. D. H. Waldeck, R. Naaman and Y. Paltiel, *APL Materials*, 2021, **9**, 040902.
6. F. Evers, A. Aharony, N. Bar-Gill, O. Entin-Wohlman, P. Hedegård, O. Hod, P. Jelinek, G. Kamieniarz, M. Lemeshko, K. Michaeli, V. Mujica, R. Naaman, Y. Paltiel, S. Refaely-Abramson, O. Tal, J. Thijssen, M. Thoss, J. M. van Ruitenbeek, L. Venkataraman, D. H. Waldeck, B. Yan and L. Kronik, *Adv. Mater.*, 2022, **34**, 2106629.
7. Y.-H. Kim, Y. Zhai, H. Lu, X. Pan, C. Xiao, E. A. Gaulding, S. P. Harvey, J. J. Berry, Z. V. Vardeny, J. M. Luther and M. C. Beard, *Science*, 2021, **371**, 1129-1133.
8. A. Chiesa, M. Chizzini, E. Garlatti, E. Salvadori, F. Tacchino, P. Santini, I. Tavernelli, R. Bittl, M. Chiesa, R. Sessoli and S. Carretta, *J. Phys. Chem. Lett.*, 2021, **12**, 6341-6347.
9. S.-H. Yang, R. Naaman, Y. Paltiel and S. S. P. Parkin, *Nat. Rev. Phys.*, 2021, **3**, 328-343.
10. A. Privitera, M. Righetto, F. Cacialli and M. K. Riede, *Adv. Opt. Mater.*, 2021, **9**, 2100215.
11. C. D. Aiello, J. M. Abendroth, M. Abbas, A. Afanasev, S. Agarwal, A. S. Banerjee, D. N. Beratan, J. N. Belling, B. Berche, A. Botana, J. R. Caram, G. L. Celardo, G. Cuniberti, A. Garcia-Etxarri, A. Dianat, I. Diez-Perez, Y. Guo, R. Gutierrez, C. Herrmann, J. Hihath, S. Kale, P. Kurian, Y.-C. Lai, T. Liu, A. Lopez, E. Medina, V. Mujica, R. Naaman, M. Noormandipour, J. L. Palma, Y. Paltiel, W. Petuskey, J. C. Ribeiro-Silva, J. J. Saenz, E. J. G. Santos, M. Solyanik-Gorgone, V. J. Sorger, D. M. Stemer, J. M. Ugalde, A. Valdes-Curiel, S. Varela, D. H. Waldeck, M. R. Wasielewski, P. S. Weiss, H. Zacharias and Q. H. Wang, *ACS Nano*, 2022, **16**, 4989-5035.
12. J. M. Abendroth, D. M. Stemer, B. P. Bloom, P. Roy, R. Naaman, D. H. Waldeck, P. S. Weiss and P. C. Mondal, *ACS Nano*, 2019, **13**, 4928-4946.
13. T. S. Metzger, S. Mishra, B. P. Bloom, N. Goren, A. Neubauer, G. Shmul, J. Wei, S. Yochelis, F. Tassinari, C. Fontanesi, D. H. Waldeck, Y. Paltiel and R. Naaman, *Angew. Chem. Int. Ed.*, 2020, **59**, 1653-1658.
14. P. C. Mondal, C. Fontanesi, D. H. Waldeck and R. Naaman, *Acc. Chem. Res.*, 2016, **49**, 2560-2568.
15. W. Mtangi, F. Tassinari, K. Vankayala, A. Vargas Jentzsch, B. Adelizzi, A. R. A. Palmans, C. Fontanesi, E. W. Meijer and R. Naaman, *JACS*, 2017, **139**, 2794-2798.
16. A. Privitera, E. Macaluso, A. Chiesa, A. Gabbani, D. Faccio, D. Giuri, M. Briganti, N. Giaconi, F. Santanni, N. Jarmouni, L. Poggini, M. Mannini, M. Chiesa, C. Tomasini, F. Pineider, E. Salvadori, S. Carretta and R. Sessoli, *Chem. Sci.*, 2022, **13**, 12208-12218.
17. S. M. Harvey and M. R. Wasielewski, *JACS*, 2021, **143**, 15508-15529.
18. T. P. Fay, *J. Phys. Chem. Lett.*, 2021, **12**, 1407-1412.
19. J. Luo and P. J. Hore, *New J. Phys.*, 2021, **23**, 043032.
20. R. Naaman, Y. Paltiel and D. H. Waldeck, *Acc. Chem. Res.*, 2020, **53**, 2659-2667.
21. T. M. Figueira-Duarte and K. Müllen, *Chem. Rev.*, 2011, **111**, 7260-7314.
22. G. Zaragoza-Galán, J. Ortíz-Palacios, B. X. Valderrama, A. A. Camacho-Dávila, D. Chávez-Flores, V. H. Ramos-Sánchez and E. Rivera, *Molecules*, 2014, **19**, 352-366.
23. M. I. Sluch, I. D. W. Samuel and M. C. Petty, *Chem. Phys. Lett.*, 1997, **280**, 315-320.
24. S. Fujii, T. Morita and S. Kimura, *Langmuir*, 2008, **24**, 5608-5614.
25. A. S. D. Sandanayaka, Y. Araki, O. Ito, G. R. Deviprasad, P. M. Smith, L. M. Rogers, M. E. Zandler and F. D'Souza, *Chem. Phys.*, 2006, **325**, 452-460.
26. M. Prato, in *Fullerenes and Related Structures*, ed. A. Hirsch, Springer Berlin Heidelberg, Berlin, Heidelberg, 1999, DOI: 10.1007/3-540-68117-5_5, pp. 173-187.
27. I. Ramirez, A. Privitera, S. Karuthedath, A. Jungbluth, J. Benduhn, A. Sperlich, D. Spoltore, K. Vandewal, F. Laquai and M. Riede, *Nat. Commun.*, 2021, **12**, 471.
28. B. C. Thompson and J. M. J. Fréchet, *Angew. Chem. Int. Ed.*, 2008, **47**, 58-77.
29. J. Niklas, S. Beaupré, M. Leclerc, T. Xu, L. Yu, A. Sperlich, V. Dyakonov and O. G. Poluektov, *J. Phys. Chem. B*, 2015, **119**, 7407-7416.
30. A. Privitera, M. Righetto, D. Mosconi, F. Lorandi, A. A. Isse, A. Moretto, R. Bozio, C. Ferrante and L. Franco, *Phys. Chem. Chem. Phys.*, 2016, **18**, 31286-31295.
31. A. Privitera, J. Grüne, A. Karki, W. K. Myers, V. Dyakonov, T.-Q. Nguyen, M. K. Riede, R. H. Friend, A. Sperlich and A. J. Gillett, *Adv. Energy Mater.*, 2022, **12**, 2103944.
32. B. P. Bloom, B. M. Graff, S. Ghosh, D. N. Beratan and D. H. Waldeck, *JACS*, 2017, **139**, 9038-9043.
33. C. Tomasini, G. Luppi and M. Monari, *JACS*, 2006, **128**, 2410-2420.
34. L. Garbuio, S. Antonello, I. Guryanov, Y. Li, M. Ruzzi, N. J. Turro and F. Maran, *JACS*, 2012, **134**, 10628-10637.
35. K. Kordatos, T. Da Ros, S. Bosi, E. Vázquez, M. Bergamin, C. Cusan, F. Pellarini, V. Tomberli, B. Baiti, D. Pantarotto, V. Georgakilas, G. Spalluto and M. Prato, *J. Org. Chem.*, 2001, **66**, 4915-4920.
36. E. M. Espinoza, J. A. Clark, J. B. Derr, D. Bao, B. Georgieva, F. H. Quina and V. I. Vullev, *ACS Omega*, 2018, **3**, 12857-12867.
37. J. F. O'Donnell and C. K. Mann, *J. electroanal. chem. interfacial electrochem.*, 1967, **13**, 157-162.
38. A. Menon, J. A. H. Dreyer, J. W. Martin, J. Akroyd, J. Robertson and M. Kraft, *Phys. Chem. Chem. Phys.*, 2019, **21**, 16240-16251.
39. B. P. Klein, L. Ruppenthal, S. J. Hall, L. E. Sattler, S. M. Weber, J. Herritsch, A. Jaegermann, R. J. Maurer, G. Hilt and J. M. Gottfried, *ChemPhysChem*, 2021, **22**, 1065-1073.
40. M. M. Islam, Z. Hu, Q. Wang, C. Redshaw and X. Feng, *Mater. Chem. Front.*, 2019, **3**, 762-781.
41. D. Genovese, E. Rampazzo, S. Bonacchi, M. Montalti, N. Zaccheroni and L. Prodi, *Nanoscale*, 2014, **6**, 3022-3036.
42. A. O. Ba-Salem and J. Duhamel, *Langmuir*, 2021, **37**, 6069-6079.
43. M. Righetto, A. Privitera, F. Carraro, L. Bolzonello, C. Ferrante, L. Franco and R. Bozio, *Nanoscale*, 2018, **10**, 11913-11922.
44. V. I. Vullev and G. Jones, *Res. Chem. Intermed.*, 2002, **28**, 795-815.
45. G. Jones Ii, X. Zhou and V. I. Vullev, *PPS*, 2003, **2**, 1080-1087.
46. C. Zuliani, F. Formaggio, L. Scipionato, C. Toniolo, S. Antonello and F. Maran, *ChemElectroChem*, 2020, **7**, 1225-1237.

47. M. Sisido, S. Hoshino, H. Kusano, M. Kuragaki, M. Makino, H. Sasaki, T. A. Smith and K. P. Ghiggino, *J. Phys. Chem. B*, 2001, **105**, 10407-10415.

48. R. A. Marcus and N. Sutin, *Biochim. Biophys. Acta*, 1985, **811**, 265-322.

49. S. S. Isied, M. Y. Ogawa and J. F. Wishart, *Chem. Rev.*, 1992, **92**, 381-394.

50. I. Ron, I. Pecht, M. Sheves and D. Cahen, *Acc. Chem. Res.*, 2010, **43**, 945-953.

51. R. Bittl and S. Weber, *Biochim. Biophys. Acta Bioenerg.*, 2005, **1707**, 117-126.

52. W. Lubitz, F. Lendzian and R. Bittl, *Acc. Chem. Res.*, 2002, **35**, 313-320.

53. H. Levanon and K. Möbius, *Annu. Rev. Biophys. Biomol. Struct.*, 1997, **26**, 495-540.

54. D. Gust, T. A. Moore and A. L. Moore, *Acc. Chem. Res.*, 1993, **26**, 198-205.

55. M. R. Wasielewski, *Chem. Rev.*, 1992, **92**, 435-461.

56. Z. E. X. Dance, Q. Mi, D. W. McCamant, M. J. Ahrens, M. A. Ratner and M. R. Wasielewski, *J. Phys. Chem. B*, 2006, **110**, 25163-25173.

57. K. Michaeli, N. Kantor-Uriel, R. Naaman and D. H. Waldeck, *Chem. Soc. Rev.*, 2016, **45**, 6478-6487.

58. Y. Liang, K. Banjac, K. Martin, N. Zigon, S. Lee, N. Vanthuyne, F. A. Garcés-Pineda, J. R. Galán-Mascarós, X. Hu, N. Avarvari and M. Lingenfelder, *Nat. Commun.*, 2022, **13**, 3356.

59. M. Kettner, V. V. Maslyuk, D. Nürenberg, J. Seibel, R. Gutierrez, G. Cuniberti, K.-H. Ernst and H. Zacharias, *J. Phys. Chem. Lett.*, 2018, **9**, 2025-2030.

60. V. Kiran, S. P. Mathew, S. R. Cohen, I. Hernández Delgado, J. Lacour and R. Naaman, *Adv. Mater.*, 2016, **28**, 1957-1962.

61. X. Li, N. Markandeya, G. Jonusauskas, N. D. McClenaghan, V. Maurizot, S. A. Denisov and I. Huc, *JACS*, 2016, **138**, 13568-13578.